Dyes and Pigments 141 (2017) 161–168

Contents lists available at ScienceDirect

Dyes and Pigments

journal homepage: www.elsevier.com/locate/dyepig

# New benzoselenadiazole-based D–A–π–A type triarylamine sensitizers for highly efficient dye-sensitized solar cells

Futai Lu [a, b, 1], Shibo Qi [c, 1], Jie Zhang [a], Guang Yang [a], Bao Zhang [a, *], Yaqing Feng [a, b, **]

[a] School of Chemical Engineering and Technology, Tianjin University, No.135, Yaguan Road, Jinnan District, Tianjin, 300350, PR China
[b] Tianjin Co-Innovation Center of Chemical Science and Engineering, Tianjin University, Tianjin, 300072, PR China
[c] School of Environmental and Chemical Engineering, Tianjin Polytechnic University, Tianjin, 300387, PR China

ARTICLE INFO

*Article history:*
Received 15 December 2016
Received in revised form
9 February 2017
Accepted 10 February 2017
Available online 13 February 2017

*Keywords:*
Dye-sensitized solar cells
Photovoltaic
Benzoselenadiazole
Triphenylamine

ABSTRACT

Three new D–A–π–A configuration organic dyes (**LC-6**, **LC-7** and **LC-8)** based on triphenylamine as the electron donor, benzoselenadiazole (BSD) as the auxiliary acceptor, either thiophene or benzene as the π spacer and cyanoacetic acid as the anchoring group have been designed and synthesized for dye-sensitized solar cells (DSCs). Introduction of octyloxy chain on the triphenylamine unit was found to be able to redshift the absorption spectra and suppress the charge recombination. It was also found that using the benzene instead of thiophene as π spacers and using CDCA coadsorbent could help to improve the $J_{sc}$ and $V_{oc}$ values of the cell. Under standard global AM 1.5 solar light conditions, a DSC employing a dye with a 1,4-phenylene unit with CDCA gave the best photovoltaic performance with a $J_{sc}$ of 13.21 mA $cm^{-2}$, a $V_{oc}$ of 734 mV, a FF of 0.69 and an overall PCE of 6.72%. These results suggest that the BSD unit can be a promising electron-withdrawing candidate in D–A–π–A type sensitizers for further exploration DSCs.



## 1. Introduction

Dye-sensitized solar cells (DSCs) have attracted considerable attention due to their distinctive advantages of low cost of production, high power conversion efficiency (PCE) and facile structural modification since the seminal report by Grätzel and coworkers [1,2]. As the key component of the DSCs, photosensitizers play an important role in light harvesting. In the past decade, researchers have devoted significant efforts to develop new and highly efficient sensitizers. The highest PCE of ruthenium complex [3], zinc porphyrins [4–10] and metal-free organic dyes [11] have reached 11.5%, 13% and 13%, respectively. Many research groups have focused on the metal-free organic sensitizers owing to their high molar extinction coefficients, good flexibility of molecular tuning, low synthetic and purification cost and tunable photophysical properties [12–17].

Most metal-free organic sensitizers are constructed with a donor-π bridge-acceptor (D-π-A) architecture for the benefit of intramolecular charge transfer (ICT) [18–20]. In 2011, the Tian group proposed a novel D-A-π-A configuration for designing a new generation of efficient and stable organic sensitizers. It was shown that introducing an additional strong electron-withdrawing group between the donor group and the π-bridge can facilitate the electron transfer, decrease the HOMO-LUMO energy gap, modulate the absorption spectra and thus result in the enhancement of the photovoltaic performance [21,22]. A series of electron-withdrawing building blocks have been successfully applied to this type of organic dyes, such as benzoxadiazole (BOD) [23,24], benzothiadiazole (BTD) [25], benzotriazole (BTZ) [26,27], quinoxaline (QN) [28,29], diketopyrrolopyrrole (DPP) [30,31], and other units. The significant role of the additional electron-withdrawing group in promoting the performance of the D-A-π-A type sensitizer-based solar cell has inspired us to search for new and more efficient additional acceptors for use in D-A-π-A dye structures.

To the best of our knowledge, benzoselenadiazole (BSe), an effective electron-withdrawing unit due to the symmetric presence of the two unsaturated nitrogen atoms, has been widely utilized as an electron-deficient unit to construct alternating D-A polymers in

* Corresponding author. School of Chemical Engineering and Technology, Tianjin University, No.135, Yaguan Road, Jinnan District, Tianjin, 300350, PR China.
** Corresponding author. School of Chemical Engineering and Technology, Tianjin University, No.135, Yaguan Road, Jinnan District, Tianjin, 300350, PR China.
*E-mail addresses:* lufutaitiger@126.com (F. Lu), boschi8000@163.com (S. Qi), zhjie@tju.edu.cn (J. Zhang), 176879931@qq.com (G. Yang), baozhang@tju.edu.cn (B. Zhang), yqfeng@tju.edu.cn (Y. Feng).
[1] These two authors contributed equally to this work.

http://dx.doi.org/10.1016/j.dyepig.2017.02.013
0143-7208/

the field of bulk heterojunction organic photovoltaics [32–34]. Moreover, the BSe unit can effectively tune the polarizability and optical and electronic properties of organic conjugated chains [35,36]. However, its application as an auxiliary acceptor in DSCs was seldom reported [37].

To further investigate the structure-properties correlations for BSe-based D-A-π-A type sensitizers for use in DSSCs, we have designed and synthesized three organic sensitizers based on the benzoselenadiazole unit, containing triphenylamine/octyltriphenylamine as donors and cyanoacrylic acid as acceptors [38–41], as shown in Fig. 1. The introduction of alkoxyl chains into the triphenylamine unit was used to prevent charge recombination due to the steric hindrance. The influence of the variation of the donor and the heterocyclic linkers (thiophene and benzene) on the optical and electrochemical properties as well as the photovoltaic performance of these dyes are systematically investigated.

## 2. Experimental

### 2.1. Materials

The synthetic routes to **LC-6, LC-7** and **LC-8** are shown in Scheme 1. All solvents and starting materials were commercially available and used without further purification (unless specially mentioned), and all reactions dealing with air- or moisture-sensitive compounds were carried out under a nitrogen atmosphere using standard Schlenk techniques. Silica gel for column chromatography was 300–400 mesh. The fluorine-doped tin oxide (FTO) conducting glass used was washed successively with detergent solution, deionized water and ethanol under ultrasonication.

### 2.2. Measurement

$^1$H NMR spectra were recorded on a Bruker AV400 MHz spectrometer in $CDCl_3$, DMSO or THF-d8 with tetramethylsilane as the internal standard. MALDI-TOF-MS was obtained with a Bruker Autoflex Tof/Tof III instrument. The UV–Vis spectra of dyes in THF solution ($3 \times 10^{-6}$ M) were measured using Shimadzu UV-1800 in 10 mm quartz cell spectrophotometer. Cyclic voltammetry (CV) measurements were carried out with a Chenhua CHI600E electrochemical analyzer at a scan rate of 50 mV/s at room temperature: a glassy carbon electrode, a Pt electrode and an $Ag/Ag^+$ electrode were used as the working electrode, counter electrode and reference electrode respectively; $Fc/Fc^+$ (ferrocene/ferrocenium) redox couple was used as an internal potential reference, and 0.1 M tetrabutylammonium perchlorate (TBAP) in anhydrous THF for the supporting electrolyte.

Commercial FTO (7 $\Omega cm^{-2}$, Hartford Glass, USA) was coated with ~8 μm thick transparent layer (DSL 18NR-T, ~20 nm, Dyesol, Australia) and ~4 μm thick scattering layer (WER2-O, 150–400 nm Dyesol, Australia) used as working electrodes. After the films were air dried for about 30 min, the samples were put into an oven for sintering using a three-stage ramp-up scheme (8 °C $min^{-1}$, 200 °C for 15 min, 350 °C for 15 min, and 550 °C for 30 min) in ambient air. The samples were then cooled to room temperature and immersed in a freshly prepared $TiCl_4$ aqueous solution (20 mM) for 0.5 h. The films were air dried and sintered again at 550 °C for 30 min. Furthermore, the films were put into the dye solution (~0.3 mM in a mixture of $CHCl_3$:EtOH = 1:1) at room temperature and kept for 12 h. The sensitized electrode was rinsed with ethanol, and dried. A sandwich cell consisting of the porphyrin-sensitized $TiO_2$ electrode as the working electrode and a Pt foil as the counter electrode was fabricated. The electrolyte solution of 0.1 M 1-propyl-2,3-dimethylimidazolium iodide (DMPII), 0.5 M 1-butyl-3-methylimidazolium iodide (BMII), 0.05 M $I_2$, 0.1 M LiI, 0.1 M guanidine thiocyanate (GuSCN), and 0.5 M *tert*-butylpyridine (TBP) in an 85/15 mixture of acetonitrile and valeronitrile were used as the redox electrolytes.

The three organic dye dye-sensitized $TiO_2$ electrodes were tested under simulated AM 1.5 irradiation (100 $mW/cm^2$) and the photocurrent density-voltage (*J-V*) characteristics were recorded on Keithley 2400 Source meter (solar AAA simulator, oriel China, calibrated with a standard crystalline silicon solar). The irradiated area of the cell was 0.159 $cm^2$, the active area of the cell is so small that no mask can be employed during the measurement. Monochromatic incident photon-to current conversion efficiency (IPCE) for the solar cells was performed on a commercial setup (Q Test Station 2000 IPCE Measurement System, CROWNTECH, USA). The monochromator was incremented through the visible spectrum to generate IPCE spectra. A white light bias (1% sunlight intensity) was applied onto the sample during the testing with an AC model (10 Hz). Electrochemical impedance spectra (EIS) were scanned in a frequency range of 0.1–106 Hz and at an AC amplitude of 10 mV at room temperature with a Chenhua CHI600E analyzer.

### 2.3. Synthesis

**Compound 2**: 4,7-dibromobenzoselenadiazole (340 mg, 1.00 mmol), $Pd(PPh_3)_4$ (100 mg, 0.087 mmol), 4-(diphenylamino) phenylboronic acid (288 mg, 1.00 mmol) and $K_2CO_3$ (1.00 g, 7.25 mmol) in toluene (40 mL) and $H_2O$ (5 mL) were heated at reflux for 12 h under a nitrogen atmosphere. After cooling to room temperature, the mixture was extracted with $CH_2Cl_2$ (3 × 50 mL). The organic portion was combined and dried over $MgSO_4$, and volatile components were removed by rotary evaporation. The residue was purified by column chromatography on silica gel ($CH_2Cl_2$/petroleum ether = 1:2, v/v) to give **2** as an orange solid (200 mg). Yield: 41.6%. $^1$H NMR (400 MHz, $CDCl_3$) δ 7.83 (d, $J$ = 7.5 Hz, 1H), 7.73 (d, $J$ = 8.7 Hz, 2H), 7.39 (d, $J$ = 7.5 Hz, 1H), 7.33 (t, $J$ = 7.6 Hz, 4H), 7.19 (dd, $J$ = 8.5, 1.9 Hz, 6H), 7.08 (t, $J$ = 7.3 Hz, 2H). MALDI-TOF-MS: $m/z$ calcd for $C_{24}H_{16}BrN_3Se$, 504.97; found, 504.83 [M+].

**Compound 3**: Compound **2** (110 mg, 0.22 mmol), $Pd(PPh_3)_4$ (100 mg, 0.087 mmol), 2-formylthiophene-5-boronic acid (31 mg, 0.22 mmol) and $K_2CO_3$ (1.00 g, 7.25 mmol) in THF (30 mL) and $H_2O$ (5 mL) were heated at reflux for 12 h. After cooling to room temperature, the mixture was extracted with $CH_2Cl_2$ (3 × 30 mL). The organic portion was combined and dried over $MgSO_4$, and volatile

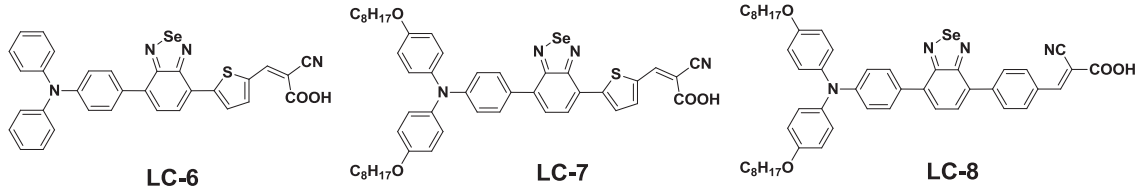


**Fig. 1.** Molecular structure of three organic sensitizers.

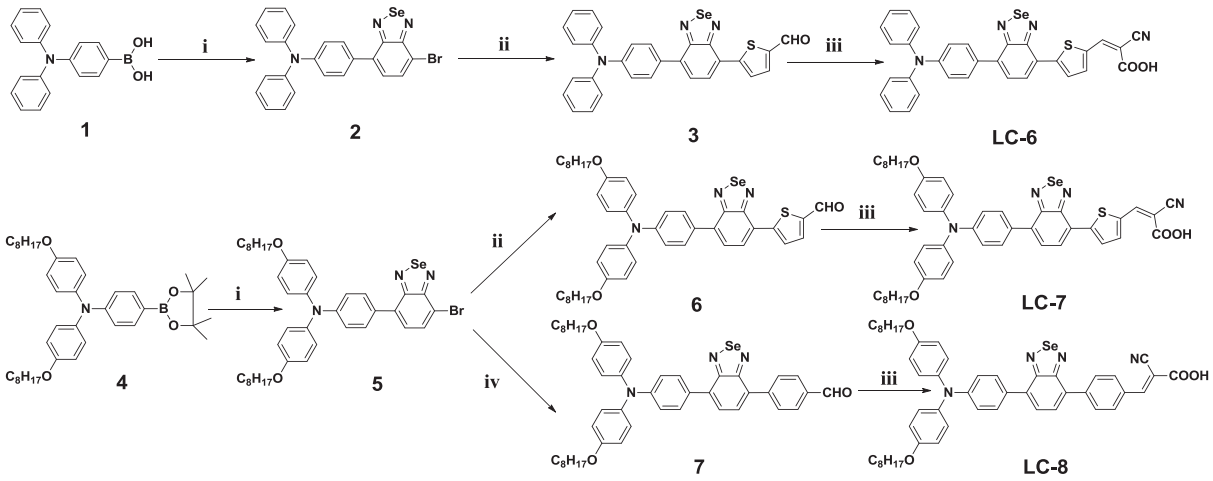

**Scheme 1.** The synthetic routes for the three dyes. Reaction conditions: i) $Pd(PPh_3)_4$, 2 M $K_2CO_3$ aqueous solution, toluene, Ar, 115 °C; ii) 2-formylthiophene-5-boronic acid, $Pd(PPh_3)_4$, 2 M $K_2CO_3$ aqueous solution, THF, Ar, 80 °C; iii) cyanoacetic acid, ammonium acetate, acetic acid, Ar, 120 °C; iv) 2-formylphenyl-5-boronic acid, $Pd(PPh_3)_4$, 2 M $K_2CO_3$ aqueous solution, THF, Ar, 80 °C.

components were removed by rotary evaporation. The residue was purified by column chromatography on silica gel ($CH_2Cl_2$/petroleum ether = 2:1, v/v) to give **3** as red solid (54 mg). Yield: 46%. $^1$H NMR (400 MHz, $CDCl_3$) δ 10.00 (s, 1H), 8.12 (d, $J$ = 3.9 Hz, 1H), 8.00 (d, $J$ = 7.4 Hz, 1H), 7.85 (dd, $J$ = 10.0, 6.2 Hz, 3H), 7.63 (s, 1H), 7.33 (t, $J$ = 7.6 Hz, 4H), 7.21 (d, $J$ = 6.6 Hz, 6H), 7.10 (s, 2H). MALDI-TOF-MS: $m/z$ calcd for $C_{29}H_{19}N_3OSe$, 537.04; found, 537.07 [M+].

**Compound LC-6**: A mixture of compound **3** (54 mg, 0.1 mmol) with cyanoacetic acid (85 mg, 1 mmol) in acetic acid (15 mL) was heated at reflux in the presence of ammonium acetate (150 mg) for 12 h under argon. After cooling the solution, water was added to quench the reaction. The precipitate was filtered and washed with water. The residue was purified by column chromatography on silica gel ($CH_2Cl_2$/ethanol = 10:1, v/v) to give a **LC-6** red solid (36 mg). Yield: 60%. Melting point: 276–278 °C. IR (KBr, $cm^{-1}$): 3429, 3031, 2217, 1682, 1584, 1562, 1492, 1415, 1382, 1322, 1247, 1196, 1108, 1082, 828, 756, 696, 510.$^1$H NMR (400 MHz, DMSO) δ 8.53 (s, 1H), 8.28–8.22 (m, 2H), 8.10 (d, $J$ = 4.2 Hz, 1H), 7.92 (d, $J$ = 8.6 Hz, 2H), 7.75 (d, $J$ = 7.5 Hz, 1H), 7.37 (t, $J$ = 7.8 Hz, 4H), 7.16–7.03 (m, 8H). $^{13}$C NMR (101 MHz, DMSO) δ 174.56, 167.29, 164.24, 158.60, 157.54, 147.96, 147.74, 147.30, 146.04, 145.35, 143.29, 143.12, 138.57, 137.57, 135.18, 132.20, 131.92, 131.29, 131.06, 130.08, 129.09, 128.03, 127.24, 125.53, 124.96, 124.02, 122.44, 118.96. MALDI-TOF-MS: $m/z$ calcd for $C_{32}H_{20}N_4O_2Se$, 604.05; found, 604.09 [M+]. HRMS-ESI($m/z$): calcd for [M−COOH]$^-$, $C_{31}H_{19}N_4SSe^-$ 559.0501; found 559.0520.

**Compound 5**: The synthesis method resembles that of compound **2**, but uses compound **4** as reagent; the compound was purified by column chromatography on silica gel ($CH_2Cl_2$/petroleum ether = 1:2, v/v) to give **5** a red solid. Yield: 37%. $^1$H NMR (400 MHz, $CDCl_3$) δ 7.82 (d, $J$ = 7.5 Hz, 1H), 7.68 (d, $J$ = 8.7 Hz, 2H), 7.36 (d, $J$ = 7.5 Hz, 1H), 7.14 (d, $J$ = 8.9 Hz, 4H), 7.03 (d, $J$ = 8.7 Hz, 2H), 6.87 (d, $J$ = 8.9 Hz, 4H), 3.96 (t, $J$ = 6.5 Hz, 4H), 1.89–1.71 (m, 4H), 1.58–1.04 (m, 16H), 1.01–0.82 (m, 6H). MALDI-TOF-MS: $m/z$ calcd for $C_{40}H_{48}BrN_3O_2Se$, 761.21; found, 761.92 [M+].

**Compound 6**: The synthesis method resembles that of compound **3**, but uses compound **5** as reagent; the compound was purified by column chromatography on silica gel ($CH_2Cl_2$/petroleum ether = 2:1, v/v) to give **6** a purple solid. Yield: 48%. [M+].$^1$H NMR (400 MHz, $CDCl_3$) δ 9.99 (s, 1H), 8.10 (d, $J$ = 4.0 Hz, 1H), 7.97 (d, $J$ = 7.4 Hz, 1H), 7.84 (d, $J$ = 4.0 Hz, 1H), 7.77 (d, $J$ = 8.7 Hz, 2H), 7.58 (d, $J$ = 7.4 Hz, 1H), 7.15 (d, $J$ = 8.9 Hz, 4H), 7.05 (d, $J$ = 8.7 Hz, 2H), 6.88 (d, $J$ = 8.9 Hz, 4H), 3.97 (t, $J$ = 6.5 Hz, 4H), 1.97–1.75 (m, 4H), 1.55–1.42 (m, 4H), 1.43–1.17 (m, 16H), 0.91 (t, $J$ = 6.7 Hz, 6H). MALDI-TOF-MS: $m/z$ calcd for $C_{45}H_{51}N_3O_3SSe$, 793.28; found, 793.01.

**Compound LC-7**: The synthesis method resembles that of compound **LC-6**, but uses compound **6** as reagent; the compound was purified by column chromatography on silica gel ($CH_2Cl_2$/$CH_3OH$ = 1:10, v/v) to give **LC-7** a purple solid. Yield: 83%. Melting point: 238–239 °C. IR (KBr, $cm^{-1}$): 3428, 3037, 2924, 2853, 2224, 1699, 1592, 1502, 1468, 1421, 1320, 1280, 1237, 1187, 1029, 826, 768, 713, 526.$^1$H NMR (400 MHz, THF) δ 8.52 (s, 1H), 8.23 (t, $J$ = 5.4 Hz, 2H), 8.09 (d, $J$ = 4.0 Hz, 1H), 7.84 (d, $J$ = 8.6 Hz, 2H), 7.69 (d, $J$ = 7.5 Hz, 1H), 7.08 (d, $J$ = 8.7 Hz, 4H), 6.93 (d, $J$ = 8.8 Hz, 4H), 6.86 (d, $J$ = 8.6 Hz, 2H), 3.94 (t, $J$ = 6.3 Hz, 4H), 1.75–1.61 (m, 4H), 1.53–1.37 (m, 4H), 1.35–1.15 (m, 16H), 0.85 (t, $J$ = 6.1 Hz, 6H). $^{13}$C NMR (101 MHz, THF) δ 173.46, 163.16, 159.02, 157.88, 156.09, 149.23,149.18, 145.53, 140.28, 137.34, 136.91, 135.99, 130.26, 129.04, 127.55, 127.34, 126.85, 125.87, 125.04, 119.01, 115.74, 115.10, 98.90, 67.83, 31.86, 29.62, 29.37, 29.27, 26.10, 22.57, 13.46. MALDI-TOF-MS: $m/z$ calcd for $C_{48}H_{52}BrN_4O_4SSe$, 860.29; found, 860.98 [M+]. HRMS-ESI($m/z$): calcd for [M-COOH]$^-$, $C_{47}H_{51}N_4O_2SSe^-$ 815.2903; found 815.2950.

**Compound 7**: The synthesis method resembles that of compound **3**, but uses compound **5** and 2-formylphenyl-5-boronic acid as reagents; The compound was purified by column chromatography on silica gel ($CH_2Cl_2$/petroleum ether = 2:1, v/v) to give **8** a red solid. Yield: 54%.$^1$H NMR (500 MHz, $CDCl_3$) δ 10.11 (s, 1H), 8.08 (d, $J$ = 8.2 Hz, 2H), 8.04 (d, $J$ = 8.3 Hz, 2H), 7.75 (d, $J$ = 8.4 Hz, 2H), 7.69 (d, $J$ = 7.2 Hz, 1H), 7.60 (d, $J$ = 7.2 Hz, 1H), 7.14 (d, $J$ = 7.9 Hz, 4H), 7.05 (d, $J$ = 8.1 Hz, 2H), 6.86 (d, $J$ = 8.8 Hz, 4H), 3.95 (t, $J$ = 6.3 Hz, 4H), 1.87–1.70 (m, 4H), 1.52–1.42 (m, 4H), 1.41–1.28 (m, 16H), 0.90 (t, $J$ = 6.8 Hz, 6H). MALDI-TOF-MS: $m/z$ calcd for $C_{47}H_{53}N_3O_3Se$, 787.33; found, 787.05 [M+].

**Compound LC-8**: The synthesis method resembles that of compound **LC-6**, but uses compound **8** as reagent; the compound was purified by column chromatography on silica gel ($CH_2Cl_2$/$CH_3OH$ = 1:10, v/v) to give **LC-8** as a red solid. Yield: 78%. Melting point: 140–142 °C. IR (KBr, $cm^{-1}$): 3438, 3036, 2922, 2852, 2220, 1682, 1568, 1501, 1469, 1415, 1323, 1286, 1240, 1202, 1104, 1044, 820, 767, 725, 530.$^1$H NMR (400 MHz, THF) δ 8.31 (s, 1H), 8.18 (q, $J$ = 8.7 Hz, 4H), 7.84 (d, $J$ = 8.8 Hz, 2H), 7.78 (d, $J$ = 7.3 Hz, 1H), 7.64 (d, $J$ = 7.3 Hz, 1H), 7.08 (d, $J$ = 8.9 Hz, 4H), 6.97 (d, $J$ = 8.8 Hz, 2H),

6.85 (d, $J$ = 8.9 Hz, 4H), 3.94 (t, $J$ = 6.4 Hz, 4H), 1.84–1.73 (m, 4H), 1.56–1.43 (m, 4H), 1.43–1.30 (m, 16H), 0.90 (t, $J$ = 6.8 Hz, 6H). $^{13}$C NMR (101 MHz, THF) δ 161.12, 157.74, 157.39, 154.16, 151.18, 147.20, 140.82, 138.55, 133.81, 129.95, 129.35, 128.75, 128.32, 128.09, 127.56, 127.16, 124.93, 124.40, 117.29, 113.62, 113.24, 101.73, 65.97, 30.00, 27.78, 27.52, 27.41, 24.24, 20.71, 11.61. MALDI-TOF-MS: $m/z$ calcd for $C_{50}H_5rN_4O_4Se$, 854.33; found, 853.99 [M+]. HRMS-ESI($m/z$): calcd for [M-COOH]$^-$, $C_{49}H_{53}N_4O_2Se^-$ 809.3339; found 809.3430.

## 3. Results and discussion

### 3.1. Synthesis

The synthesis of the three organic sensitizers is depicted in Scheme 1. The synthesis of the three target sensitizers started from 2,5-dibromobenzoselenadiazole which was firstly converted to compounds **2** and **5** via stepwise Suzuki coupling with either 4-(diphenylamino)phenylboronic acid (**1**) or 4-(octyloxy)-*N*-(4-(octyloxy)phenyl)-*N*-(4-(4,4,5,5-tetramethyl-1,3,2-dioxaborolan-2-yl)phenyl)aniline (**4**), respectively. Further Suzuki coupling with either 2-formylthiophene-5-boronic acid or 4-formybenzene-5-boronic acid introduced the π-spacer. The precursors **3**, **6** and **7** were then converted to the final sensitizers **LC-6**, **LC-7** and **LC-8** by Knoevenagel condensation with cyanoacetic acid. Compared to **LC-6**, octyloxy substituted triphenylamino group in **LC-7** and **LC-8** as the electron donor not only provided stronger electron donating capability, resulting in the enhancement of the light harvesting capacity, but also form an aliphatic network, which increases the distance between $TiO_2$ surface and the electrolyte, thus suppressing the adverse charge recombination between photo-injected electrons and $I_3^-/I_2$, which may improve the $V_{oc}$ [42].

### 3.2. Photophysical properties

The absorption spectra of **LC-6**, **LC-7** and **LC-8** in EtOH and on the $TiO_2$ film are shown in Fig. 2. The corresponding data are summarized in Table 1. The UV–vis spectra of the three sensitizers exhibit two major absorption bands: the former at 300–400 nm can be ascribed to the π-π* transition from the triphenylamine to the BSD moiety, and the latter at 450–550 nm is attributed to the intramolecular charge transfer (ICT) from the eletron-donating unit of triphenylamine to the cyanoacetic acid acceptor unit [43]. A comparison of the absorption spectra of **LC-6** and **LC-7** suggested that upon introducing the octyloxy chains in the triphenylamine, the maximum absorption band red-shifted by 19 nm and the molar extinction coefficient is increased. The reason behind the absorption red-shift is that the octyloxy chains can increase the π-conjugation length via enhanced electron delocalization over the entire electron-donating moiety, which results in the lower band gap and red-shifted absorption spectra [44,45]. On the contrary, the 34 nm hypochromic shift of **LC-8** compared to **LC-7** is mainly caused by the higher tendency of thiophene compared to benzene to form quinoid structure, which is in favor of electronic resonance [46,47]. The absorption spectra of the three sensitizers adsorbed on the $TiO_2$ film also display two major absorption bands, but the bands are significantly broadened and red-shifted when compared with the corresponding solution spectra, indicating the formation of *J*-aggregation of the dyes on the $TiO_2$ surface [48] (see Fig. 3).

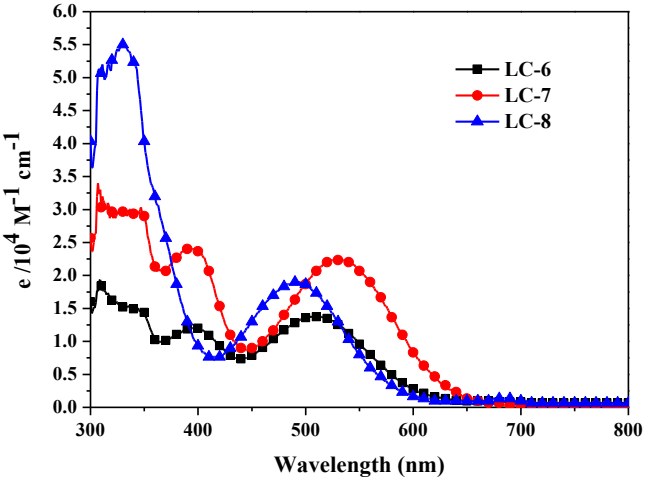


**Fig. 2.** UV–visible absorption spectra of the three dyes in THF ($3.0 \times 10^{-6}$ M).

### 3.3. Electrochemical properties

The electronic properties of the three organic sensitizers were investigated by cyclic voltammery (CV). The corresponding data are listed in Table 1 and Fig. S10. All the three organic sensitizers show a quasi-reversible one-electron oxidation couple which can be ascribed to the oxidation of the triphenylamine. The redox potentials ($E_{ox}$) of **LC-6**, **LC-7** and **LC-8** corresponding to the HOMO energy level are located at 1.16, 0.90 and 0.91 V, respectively. The HOMO level of **LC-6** is higher than that of **LC-7** and **LC-8** due to the stronger electron-donating ability as the incorporation of the alkoxy chains in the latter. As well known, the HOMO level lies predominantly on the donor moiety of the molecule, so that **LC-7** and **LC-8** containing the same donor unit have the similar HOMO levels. The values of HOMO levels are all more positive than the energy level of $I^-/I_3^-$ redox (0.4 V vs NHE) [49] guaranteeing the dye regeneration. The $E_{0\text{-}0}$ (zero-zero transition energies) of the three sensitizers are 2.04, 1.97 and 2.13 V, respectively, which are calculated from the onset wavelength of the absorption spectra. The estimated excited-state potential corresponding to the LUMO levels calculated from $E_{HOMO}$ to $E_{0\text{-}0}$, are −0.88, −1.07 and −1.22 V, respectively, which are more negative than the conduction band edge energy level of the $TiO_2$ semiconductor (−0.5 V vs NHE) [50], ensuring the efficient driving force for electron injection from the excited state of the dyes into the $TiO_2$ electrode.

### 3.4. Theoretical approach

Density functional theory (DFT) calculations were carried out to obtain further insight into the geometrical configuration and electron distribution of the frontier orbitals of the three dyes. Structural optimizations and subsequent frequency calculations for **LC-6**, **LC-7** and **LC-8** were carried out by using the B3LYP functional with the 6-311G* basis set as implemented in the Gaussian 09 suite of programs [51]. The polarizable continuum model (PCM) was employed in the optimization with THF as the solvent. All the octyloxy groups have been replaced with methoxy groups to save calculation time. As shown in the optimized conformation (Fig. S11), the dihedral angles between the triphenylamine and the additional acceptor BSD for **LC-6**, **LC-7** and **LC-8** are 33.76°, 32.73° and 34.59°, respectively. The dihedral angles between the BSD unit and the neighboring thiophene and phenyl ring are 1.13°, 0.97° and 34.28°, respectively. The relative smaller torsion angle for thiophene-bridged **LC-6** and **LC-7** ensures a good molecular coplanarity to keep high electronic communication with respect to phenylene-bridged **LC-8**, leading to the larger red-shift in absorption band in solution and the additional absorption band at around 400 nm.

Figs. 4 and 5 show the calculated frontier molecular orbital and their corresponding energies and the HOMO and LUMO gaps of the

**Table 1**
Photophysical properties of the three sensitizers.

| Dye | $\lambda_{max}$ (nm ($\varepsilon$/$10^3$ $M^{-1}$ $cm^{-1}$))[a] | $\lambda_{max}$/nm[b] | HOMO (V)[c] | $E_{0\text{-}0}$(V)[d] | LUMO (V)[e] |
|---|---|---|---|---|---|
| **LC-6** | 392(12,000),503(13,733) | 517 | 1.16 | 2.04 | −0.88 |
| **LC-7** | 389 (24,000),522(22,333) | 552 | 0.90 | 1.97 | −1.07 |
| **LC-8** | 332(55,000),488(19,000) | 495 | 0.91 | 2.13 | −1.22 |

[a] Absorption data were obtained in THF solution ($3 \times 10^{-6}$ M).
[b] Absorption maximum on $TiO_2$ film.
[c] HOMO potentials measured vs $Fc^+$/Fc were converted to those vs. the normal hydrogen electrode (NHE) by addition of +0.63 V.
[d] $E_{0\text{-}0}$ values were calculated from the onset wavelength of the absorption spectra in solution.
[e] The LUMO was calculated with the expression of LUMO = HOMO − $E_{0\text{-}0}$.

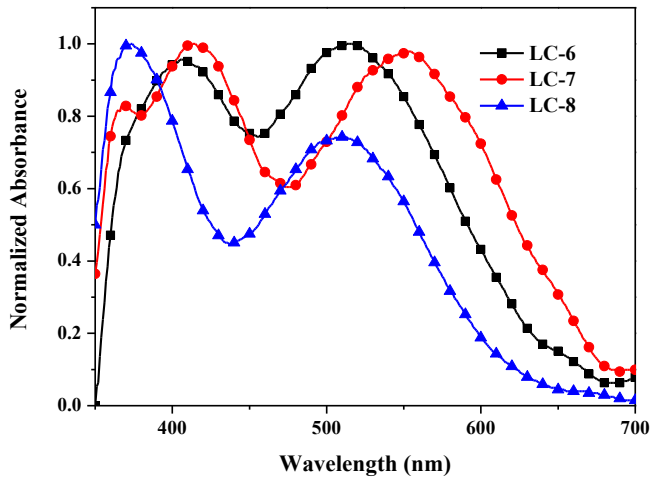


**Fig. 3.** UV–Visible absorption spectra of the $TiO_2$ films.

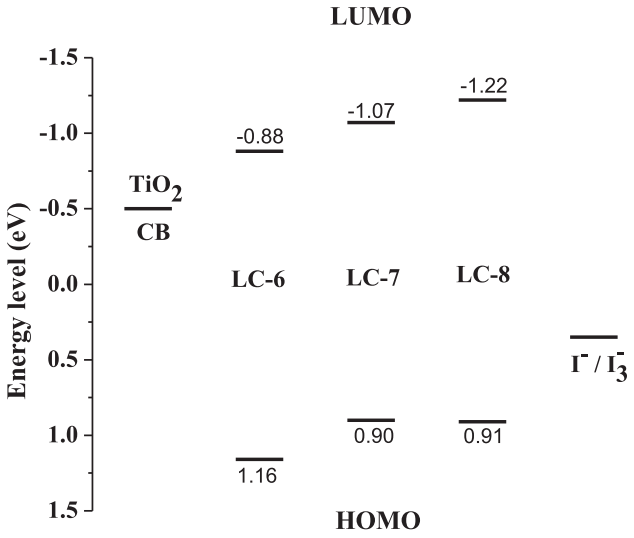


**Fig. 4.** Energy level (eV) of HOMO and LUMO molecular orbitals for the three sensitizers.

three organic dyes **LC-6, LC-7** and **LC-8**. It is found that the electron density is predominately distributed at the triphenylamine unit for the HOMO orbital, while for the LUMO orbital, electrons are located on the BSD and cyanoacrylate units. Here, the electrons can successively transfer from the donor to BSD, then transfer to the anchor (cyanoacetic acid) and finally inject into $TiO_2$ film. Furthermore, attaching the octyloxy groups significantly extends the π-conjugation of the donor, which arises the HOMO energy and facilitates the oxidation. When the thiophene spacer was replaced by phenylene, the LUMO energy level and the band gap of **LC-8** were both increased. As a consequence, **LC-7** exhibits the lowest HOMO-LUMO energy gap (1.86 eV) among all dyes, resulting in the red shift of the absorption spectra. The simulated absorption spectra based on DFT calculation (Fig. S12) show qualitative agreement with experimental results, albeit the excitation energies are overestimated. The corresponding data are summarized in Table S1. The results suggest that the former band at 300–400 nm can be ascribed to the local excitation of the organic dye, and the latter at 450–550 nm is attributed to the $S_0 \rightarrow S_1$ excitation.

### 3.5. Photovoltaic performance of DSSCs

The photovoltaic performance of DSSCs were measured under standard AM 1.5 irradiation (100 mW $cm^{-2}$) and the detailed parameters of short-circuit current density ($J_{sc}$), open-circuit voltage ($V_{oc}$), fill factor (FF) and power conversion efficiency (PCE) are listed in Table 2. The photocurrent density-voltage (*J-V*) curves are displayed in Fig. 6. The DSSC based on **LC-6** exhibited photovoltaic performance with a $J_{sc}$ of 7.87 mA $cm^{-2}$, a $V_{oc}$ of 585 mV, and a FF of 0.72, corresponding to a PCE of 3.33%. Upon incorporation of the alkoxy chains in the triphenylamine, the resultant **LC-7**-based cell showed an improvement of $V_{oc}$ (598 mV) and finally gave a higher PCE of 3.46% with a FF of 0.74. A plausible explanation is that the two octyloxy chains substituted on the triphenylamine of **LC-7** are beneficial to form a blocking layer which limits the electron recombination, and hence increases the electron lifetime and the $V_{oc}$. Notably, when the thiophene-bridge of **LC-7** was replaced by benzene, the **LC-8**-based DSSC displayed a higher PCE of 4.11% with an increased $J_{sc}$ (8.59 mA $cm^{-2}$) and $V_{oc}$ (687 mV). It should be pointed out that less planar skeleton of benzene can effectively suppress the dark current and reduce the electron recombination, resulting in a higher $V_{oc}$ [52]. The measured dye loading values for **LC-6**, **LC-7** and **LC-8** are close ($0.94 \times 10^{-7}$ mol $cm^2$, $0.82 \times 10^{-7}$ mol $cm^2$ vs $0.88 \times 10^{-7}$ mol $cm^2$), indicating that the improved $J_{sc}$ for **LP-8** is not resulted from the dye loading amount. It is believed that one reason might be that the replacement of benzene has the more negative LUMO energy level than the conduction band of $TiO_2$, providing greater driving force for charge injection. Furthermore, as we know, sensitizer aggregation at the $TiO_2$ surface could induce the excited state quenching, and thus the less planar conformation of **LC-8** will ease the aggregation, leading to more efficient electron injection.

In order to prevent the unfavorable aggregation of dye molecules and retard charge recombination, a common and effective strategy is to use CDCA as coadsorbent due to its nonplanar and bulky configuration. In this work, 20 mM CDCA were added during dye soaking of the three sensitizers. From Table 2, we can find that both the $J_{sc}$ and $V_{oc}$ values increased, indicating that CDCA had successfully disrupt the aggregation and retard charge recombination between $TiO_2$ and electrolyte. The best PCE have increased to

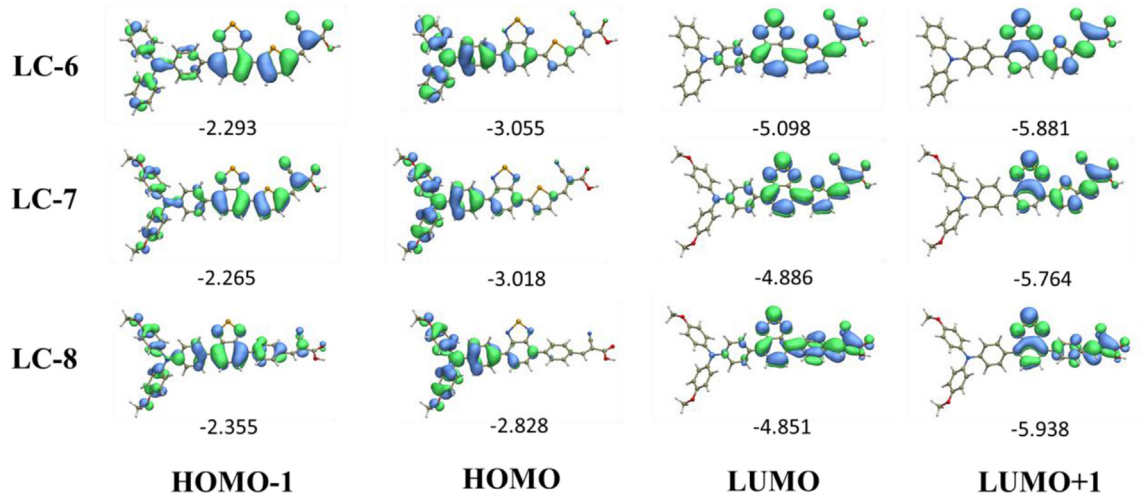


**Fig. 5.** Molecular orbital distributions and energy levels of the three dyes.

**Table 2**
Photovoltaic parameters of porphyrin-sensitized solar cells.

| Dye | $J_{sc}$/mA cm$^2$ | $V_{oc}$/mV | FF | η/% |
|---|---|---|---|---|
| **LC-6** | 7.87 | 585 | 0.72 | 3.33 |
| **LC-6** + **CDCA** | 9.98 | 620 | 0.74 | 4.59 |
| **LC-7** | 7.84 | 598 | 0.74 | 3.46 |
| **LC-7** + **CDCA** | 10.82 | 628 | 0.73 | 4.99 |
| **LC-8** | 8.59 | 687 | 0.69 | 4.11 |
| **LC-8** + **CDCA** | 13.21 | 734 | 0.69 | 6.72 |
| **N719**[a] | 14.89 | 770 | 0.67 | 7.65 |

[a] As a reference, the overall efficiency of N719 sensitized solar cells was determined.

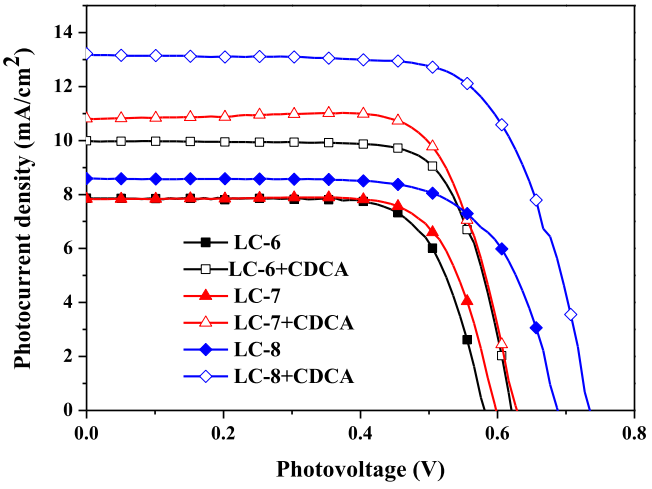


**Fig. 6.** *J-V* curves of DSSCs based on the three dyes.

6.72% based on **LC-8** sensitized cell, with a $J_{sc}$ of 13.21 mA cm$^{-2}$, a $V_{oc}$ of 734 mV, and a FF of 0.69, reaching about 87% of the value of that for an **N719**-based cell fabricated and measured under the same condition.

The incident photon-to-current conversion efficiency (IPCE) as a function of incident wavelength for DSSCs based on **LC-6, LC-7** and **LC-8** with or without CDCA are shown in Fig. 7. It can be clearly seen that the IPCE responses are in the range of 300–730 nm for **LC-6**,

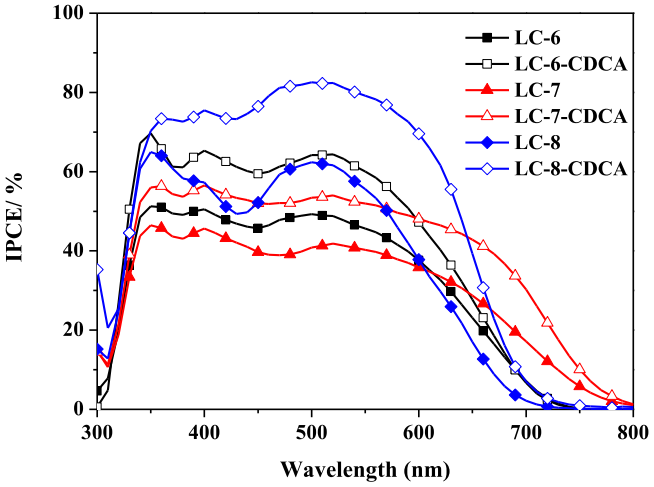


**Fig. 7.** Typical action spectra of IPCE obtained for solar cells sensitized by the three dyes.

300–800 nm for **LC-7** and 300–700 nm for **LC-8**, respectively. Unfortunately, even though the IPCE response of **LC-7** is the broadest, IPCE values are the lowest with the plateau no more than 50%, which is consistent with the lowest $J_{sc}$. The IPCE values of **LC-8** are much higher at the range of 400–600 nm and have reached over 60% at 520 nm, which could explain the corresponding higher $J_{sc}$ value for **LC-8**-based cell in spite of the narrower IPCE response compared to **LC-6** and **LC-7**. Interestingly, the IPCE values of the three dyes with CDCA coabsorbent are much improved compared to those without CDCA, which indicated that the aggregation was indeed suppressed, thus resulting in more charge collection and the greater $J_{sc}$. The IPCE values of the cell based on **LC-8** with CDCA achieved over 70% from 350 to 600 nm with the highest IPCE value of 82% at 520 nm, which ensured the highest $J_{sc}$ values among all the three dye-based cells.

Electrochemical impedance spectroscopy (EIS) of DSSCs were obtained under −0.6 V in the dark to investigate the electron recombination. The Nyquist plots for DSSCs based on **LC-6**, **LC-7** and **LC-8** are shown in Fig. 8 and the Bode plots shown in Fig. 9. The larger semicircle in the Nyquist plots, indicates the larger resistance of charge transfer ($R_{ct}$) from $TiO_2$ to the electrolyte. As we know, a

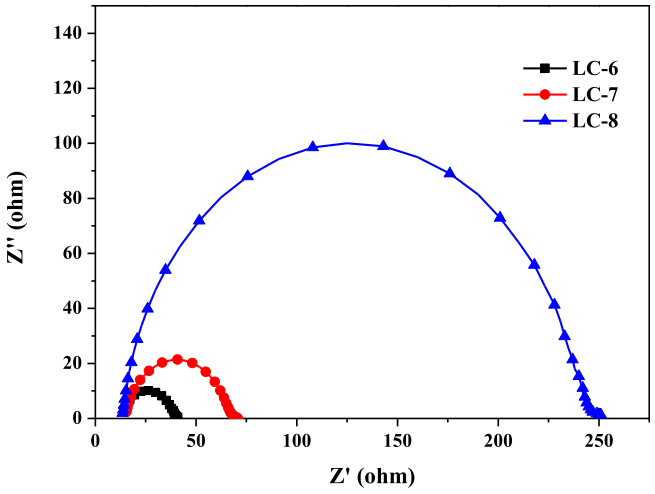


**Fig. 8.** Nyquist plots of electrochemical impedance spectra measured at a forward bias of −0.6 V under dark conditions for the DSSCs.

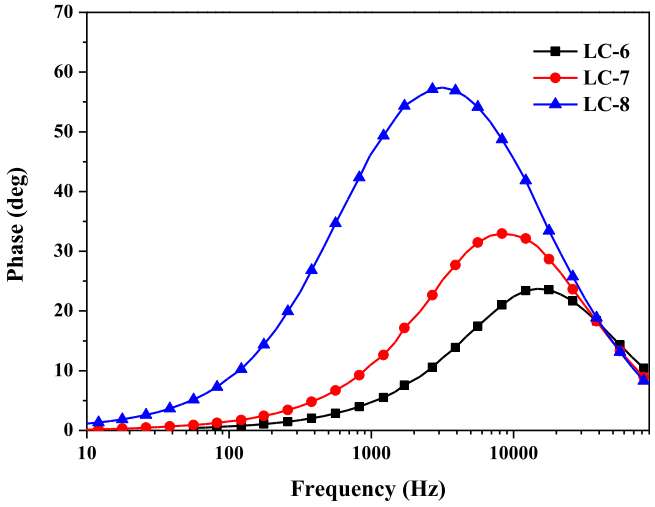


**Fig. 9.** Bode-phase plots of electrochemical impedance spectra measured at a forward bias of −0.6 V under dark conditions for the DSSCs.

larger $R_{ct}$ means the reduced electron recombination in the cells and therefore an improved photovoltage [53,54]. The lager semicircle of the **LC-8** cell than those of **LC-6** and **LC-7**, indicated a strongly reduced electron recombination, which is consistent with the largest $V_{oc}$ values of the **LC-8** cell.

In the Bode phase plots (Fig. 9), the reciprocal of frequency peak is regarded as the electron lifetime as it represents the charge-transport process of injected electrons in $TiO_2$. Electron lifetime ($\tau_e$) can be calculated from the peak frequency ($f$) in the Bode plots using $\tau_e = 1/(2\pi f)$ [55]. The peaks in Bode plots of the three cells were found to be in the order **LC-8** < **LC-7** < **LC-6**, and thus the electron lifetime were to increase in the order **LC-6** < **LC-7** < **LC-8**, explaining the increased $V_{oc}$ from **LC-6** to **LC-7** and **LC-8**. From the EIS analysis, it can be found that the resistance of charge recombination and the electron lifetime are increased in the order **LC-6** < **LC-7** < **LC-8**, indicating that the introduction of alkoxy chains at the triphenylamine donor moiety and the use of benzene instead of thiophene are effective ways to modify the $TiO_2$/dye/electrolyte interface and increase $V_{oc}$ of the corresponding DSSCs.

## 4. Conclusions

In summary, three new D-A-π-A organic dyes with triphenylamine/octyltriphenylamine as donor, either thiophene or 1,4-phenylene as the linker, benzoselenadiazole (BSD) and cyanoacrylic acid as the acceptor, were successfully designed and synthesized. The influence of the variation of the donor and the π spacer on the optical and electrochemical properties of these dyes as well as the photovoltaic performance of the corresponding solar cells is systematically investigated. The results showed that attaching the octyloxy chain to the donor is proved to be an effective strategy to suppress the adverse charge recombination and improve the $V_{oc}$ values. Moreover, the use of phenyl π-spacer rather than thiophene moiety and adding CDCA coadsorbent could help to improve the $J_{sc}$ and $V_{oc}$ values of the cells. Hence, the **LC-8** based DSSC with CDCA coadsorbent gave the best photovoltaic performance with a $J_{sc}$ of 13.21 mA $cm^{-2}$, a $V_{oc}$ of 734 mV, a FF of 0.69 and an overall PCE of 6.72%. These results reveal that **BSD** can be a promising electron-withdrawing group and thus an additional acceptor to construct effective D-A-π-A type organic sensitizers for use in DSSCs.

## Acknowledgment

This work was supported by National Natural Science Foundation of China (No. 21476162). The acknowledgment is also extended to International S&T Cooperation Project of China (No. 2012DFG41980, 2016YFE0114900).

## Appendix A. Supplementary data

Supplementary data related to this article can be found at http://dx.doi.org/10.1016/j.dyepig.2017.02.013.

## References

[1] Dresselhaus MS, Thomas IL. Alternative energy technologies. Nature 2001;414:332–7.
[2] O'Regan B, Grätzel M. A low-cost, high-efficiency solar cell based on dye-sensitized colloidal $TiO_2$ films. Nature 1991;353:737–40.
[3] Grätzel M. Photoelectrochemical cells. Nature 2001;414:338–44.
[4] Chen CY, Wang MK, Li JY, Pootrakulchote N, Alibabaei L, Ngocle Ch, et al. Highly efficient light-harvesting ruthenium sensitizer for thin-film dye-sensitized solar cells. ACS Nano 2009;3:3103–9.
[5] Mathew S, Yella A, Gao P, Humphry-Baker R, Curchod BFE, Ashari-Astani N, et al. Dye-sensitized solar cells with 13% efficiency achieved through the molecular engineering of porphyrin sensitizers. Nat Chem 2014;6:242–7.
[6] Urbani M, Grätzel M, Nazeeruddin MK, Torres T. Meso-substituted porphyrins for dye-sensitized solar cells. Chem Rev 2014;114:12330–96.
[7] Xie YS, Tang YY, Wu WJ, Wang YQ, Liu JC, Li X, et al. Porphyrin cosensitization for a photovoltaic efficiency of 11.5%: a record for non-Ruthenium solar cells based on iodine electrolyte. J Am Chem Soc 2015;137:14055–8.
[8] Tang Y, Wang Y, Li X, Ågren H, Zhu WH, Xie Y. Porphyrins containing a triphenylamine donor and up to eight alkoxy chains for dye-sensitized solar cells: a high efficiency of 10.9%. ACS Appl Mater Interfaces 2015;7:27976–85.
[9] Wang Y, Chen B, Wu W, Li X, Zhu WH, Tian H, et al. Efficient solar cells sensitized by porphyrins with an extended conjugation framework and a carbazole donor: from molecular design to cosensitization. Angew Chem Int Ed 2014;53:10779–83.
[10] Wei T, Sun X, Li X, Ågren H, Xie Y. Systematic investigations on the roles of the electron acceptor and neighboring ethynylene moiety in porphyrins for dye-sensitized solar cells. ACS Appl Mater Interfaces 2015;7:21956–65.
[11] Wang Y, Li X, Liu B, Wu W, Zhu W, Xie Y. Porphyrins bearing long alkoxyl chains and carbazole for dye-sensitized solar cells: tuning cell performance through an ethynylene bridge. RSC Adv 2013;3:14780–90.
[12] Yao Z, Wu H, Yang L, Wang JT, Zhang J, Zhang M, et al. Dithienopicenocarbazole as the kernel module of low-energy-gap organic dyes for efficient conversion of sunlight to electricity. Energy Environ Sci 2015;8:3192–7.
[13] Wu YZ, Marszalek M, Zakeeruddin SM, Zhang Q, Tian H, Grätzel M, et al. High-conversion-efficiency organic dye-sensitized solar cells: molecular engineering on D-A-π-A featured organic indoline dyes. Energy Environ Sci 2012;5:8261–72.
[14] Lu X, Feng Q, Lan T, Zhou G, Wang ZS. Molecular engineering of quinoxaline-based organic sensitizers for highly efficient and stable dye-sensitized solar

cells. Chem Mater 2012;24:3179–87.
[15] Liang M, Chen J. Arylamine organic dyes for dye-sensitized solar cells. Chem Soc Rev 2013;42:3453–88.
[16] Wu JH, Li GF, Zhang L, Zhou G, Wang ZS. Energy level engineering of thieno [3,4-b]pyrazine based organic sensitizers for quasi-solid-state dyesensitized solar cells. J Mater Chem A 2016;4:3342–55.
[17] Li XG, Zheng ZW, Jiang W, Wu WJ, Wang ZH, Tian H. New D–A–π–A organic sensitizers for efficient dye-sensitized solar cells. Chem Commun 2015;51: 3590–2.
[18] Yang JB, Ganesan P, Teuscher J, Moehl T, Kim YJ, Yi CY, et al. Influence of the donor size in D-π-A organic dyes for dye-sensitized solar cells. J Am Chem Soc 2014;136:5722–30.
[19] Haid S, Marszalek M, Mishra A, Wielopolski M, Teuscher J, Moser JE, et al. Significant improvement of dye-sensitized solar cell performance by small structural modification in π-conjugated donor–acceptor dyes. Adv Funct Mater 2012;22:1291–302.
[20] Mishra A, Fischer MKR, Bäuerle P. Metal-Free organic dyes for dye-sensitized solar cells: from structure: property relationships to design rules. Angew Chem Int Ed 2009;48:2474–99.
[21] Hagfeldt A, Boschlo G, Sun L, Kloo L, Pettersson H. Dye-sensitized solar cells. Chem Rev 2010;110:6595–663.
[22] Wu YZ, Zhu WH, Zakeeruddin SM, Grätzel M. Insight into D-A-π-A structured sensitizers: a promising route to highly efficient and stable dye-sensitized solar cells. ACS Appl Mater Interfaces 2015;7:9307–18.
[23] Wu YZ, Zhu WH. Organic sensitizers from D-π-A to D-A-π-A: effect of the internal electron-withdrawing units on molecular absorption, energy levels and photovoltaic performances. Chem Soc Rev 2013;42:2039–58.
[24] Zhu HB, Wu YZ, Liu JC, Zhang WW, Wu WJ, Zhu WH. D-A-π-A featured sensitizers containing an auxiliary acceptor of benzoxadiazole: molecular engineering and co-sensitization. J Mater Chem A 2015;3:10603–9.
[25] Wu YZ, Zhang X, Li WQ, Wang ZS, Tian H, Zhu WH. Hexylthiophene-featured D-A-π-A structural indoline chromophores for coadsorbent-free and panchromatic dye-sensitized solar cells. Adv Energy Mater 2012;2:149–56.
[26] Zhu HB, Li WQ, Wu YZ, Liu B, Zhu SQ, Li X, et al. Insight into benzothiadiazole acceptor in D-A-π-A configuration on photovoltaic performances of dye-sensitized solar cells. ACS Sustain Chem Eng 2014;2:1026–34.
[27] Chai QP, Li WQ, Wu YZ, Pei K, Liu JC, Geng ZY, et al. Effect of a long alkyl group on cyclopentadithiophene as a conjugated bridge for D-A-π-A organic sensitizers: IPCE, electron diffusion length, and charge recombination. ACS Appl Mater Interfaces 2014;6:14621–30.
[28] Cui Y, Wu YZ, Lu XF, Zhang X, Zhou G, Miapeh FB, et al. Incorporating benzotriazole Moiety to construct D-A-π-A organic sensitizers for solar cells: significant enhancement of open-circuit photovoltage with long alkyl group. Chem Mater 2011;23:4394–401.
[29] Pei K, Wu YZ, Islam A, Zhu SQ, Han LY, Geng ZY, et al. Dye-sensitized solar cells based on quinoxaline dyes: effect of π-linker on absorption, energy levels, and photovoltaic performances. J Phys Chem C 2014;118:16552–61.
[30] Pei K, Wu YZ, Li H, Geng ZY, Tian H, Zhu WH. Cosensitization of D-A-π-A quinoxaline organic dye: efficiently filling the absorption valley with high photovoltaic efficiency. ACS Appl Mater Interfaces 2015;7:5296–304.
[31] Ganesan P, Yella A, Holcombe TW, Gao P, Rajalingam R, Al-Muhtaseb SA, et al. Unravel the impact of anchoring groups on the photovoltaic performances of diketopyrrolopyrrole sensitizers for dye-sensitized solar cells. ACS Sustain Chem Eng 2015;3:2389–96.
[32] Tian gj, Cai SY, Li X, Ågren H, Wang QC, Huang JH, et al. A new D-A-π-A type organic sensitizer based on substituted dihydroindolo [2,3-b] carbazole and DPP unit with a bulky branched alkyl chain for highly efficient DSCs. J Mater Chem A 2015;3:3777–84.
[33] Poverenov E, Zamoshchik N, Patra A, Ridelman Y, Bendikov M. Unusual doping of donor–acceptor-type conjugated polymers using lewis acids. J Am Chem Soc 2014;136:5138–49.
[34] Pati PB, Das S, Zade SS. Benzooxadiazaole-based D-A-D co-oligomers: synthesis and electropolymerization. J Polym Sci Part A Polym Chem 2012;50: 3996–4003.
[35] Elsawy W, Kang HK, Yu K, Elbarbary A, Lee K, Lee JS. Synthesis and characterization of isoindigo-based polymers using CH-arylation polycondensation reactions for organic photovoltaics. J Polym Sci Part A Polym Chem 2014;52: 2926–33.
[36] Das S, Zade SS. Poly(cyclopenta[*c*]selenophene): a new polyselenophene. Chem Commun 2010;46:1168–70.
[37] Haid S, Mishra A, Uhrich C, Pfeiffer M, Bauerle P. Dicyanovinylene-substituted selenophenethiophene co-oligomers for small-molecule organic solar cells. Chem Mater 2011;23:4435–44.
[38] Velusamy M, Justin Thomas KR, Lin JT, Hsu YC, Ho KC. Organic Dyes incorporating low-band-gap chromophores for dye-sensitized solar cells. Org Lett 2005;7:1899–902.
[39] Liyanage NP, Yella A, Nazeeruddin M, Grätzel M, Delcamp JH. Thieno[3,4-b] pyrazine as an electron deficient π-bridge in D-A-π-A DSCs. ACS Appl Mater Interfaces 2016;8:5376–84.
[40] Zhu HB, Liu B, Liu JC, Zhang WW, Zhu WH. D-A-π-A featured sensitizers by modification of auxiliary acceptor for preventing "trade-off" effect. J Mater Chem C 2015;3:6882–90.
[41] Mao JY, Guo FL, Ying WJ, Wu WJ, Li J, Hua JL. Benzotriazole-bridged Sensitizers containing a furan moiety for dye-sensitized solar cells with high open-circuit voltage performance. Chem Asian J 2012;7:982–91.
[42] Irie S, Fuse S, Maitani MM, Wada Y, Ogomi Y, Hayase S, et al. Rapid synthesis of D-A-π-A dyes through a one-pot three- component suzuki-miyaura coupling and an evaluation of their photovoltaic properties for use in dye-sensitized solar cells. Chem Eur J 2016;22:2507–14.
[43] Wang J, Liu K, Ma L, Zhan X. Triarylamine: versatile platform for organic, dye-sensitized, and perovskite solar cells. Chem Rev 2016;116:14675–725.
[44] Ning Z, Fu Y, Tian H. Improvement of dye-sensitized solar cells: what we know and what we need to know. Energy Environ Sci 2010;3:1170–81.
[45] Ying WJ, Yang JB, Wielopolski M, Moehl T, Moser JE, Comte P, et al. New pyrido[3,4-*b*]pyrazine-based sensitizers for efficient and stable dye-sensitized solar cells. Chem Sci 2014;5:206–14.
[46] Yen YS, Ni JS, Hung WI, Hsu CY, Chou HH, Lin JT. Naphtho[2,3-*c*][1,2,5]thiadiazole and 2H-naphtho[2,3-*d*][1,2,3]triazole-containing D-A-π-A conjugated organic dyes for dye-sensitized solar cells. ACS Appl Mater Interfaces 2016;8: 6117–26.
[47] Hansch C, Leo A, Taft RW. A survey of hammett substituent constants and resonance and field parameters. Chem Rev 1991;91:165–95.
[48] Duan XM, Konami H, Okada S, Matsuda H, Nakanishi H, Oikawa H. Second-order hyperpolarizabilities of stilbazolium cations studied by semiempirical calculation. J Phys Chem 1996;100:17780–5.
[49] Zhu WH, Wu YZ, Wang ST, Li WQ, Li X, Chen J, et al. Organic D-A-π-A solar cell sensitizers with improved stability and spectral response. Adv Funct Mater 2011;21:756–63.
[50] Hagfeldt A, Grätzel M. Light-induced redox reactions in nanocrystalline systems. Chem Rev 1995;95:49–68.
[51] Hara K, Sato T, Katoh R, Furube A, Ohga Y, Shinpo A, et al. Molecular design of coumarin dyes for efficient dye-sensitized solar cells. J Phys Chem B 2003;107:597–606.
[52] Rassolov VA, Pople JA, Ratner MA, Windus TL. 6-31G* basis set for atoms K through Zn. J Chem Phys 1998;109:1223–9.
[53] Ying WJ, Guo FL, Li J, Zhang Q, Wu WJ, Tian H, et al. Series of new D-A-π-A organic broadly sbsorbing sensitizers containing isoindigo unit for highly efficient dye-sensitized solar cells. ACS Appl Mater Interfaces 2012;4: 4215–24.
[54] Qian X, Lu L, Zhu YZ, Gao HH, Zheng JY. Phenothiazine-functionalized push–pull Zn porphyrin photosensitizers for efficient dye-sensitized solar cells. RSC Adv 2016;6:9057–65.
[55] Wang Z, Wang H, Liang M, Tan Y, Cheng F, Sun Z, et al. Judicious design of indoline chromophores for high-efficiency iodine-free dye-sensitized solar cells. ACS Appl Mater Interfaces 2014;6:5768–78.